Multiscale simulation of porcelain tiles manufacturing

C. L. Alves [1], Agenor De Noni Jr [2], R. Janssen [3], D. Hotza [2,4], J.B. Rodrigues Neto [4], S.Y. Gómez González [2], S. Heinrich [1], M. Dosta [1]

(1) Institute of Solids Process Engineering and Particle Technology, Hamburg University of Technology (TUHH), 21073 Hamburg, Germany

(2) Department of Chemical Engineering (EQA), Federal University of Santa Catarina (UFSC), 88040-900 Florianópolis, SC, Brazil

(3) Institute of Advanced Ceramics, Hamburg University of Technology (TUHH), 21073 Hamburg, Germany

(4) Graduate Program in Materials Science and Engineering (PGMAT), Federal University of Santa Catarina (UFSC), 88040-900 Florianópolis, SC, Brazil

1.0 Introduction

Porcelain stoneware is produced by a sequence of processing steps connected by material and energy flows on a "wet" or "dry" configuration. Fig. 1 shows the wet route configuration with the most relevant energy and material streams.

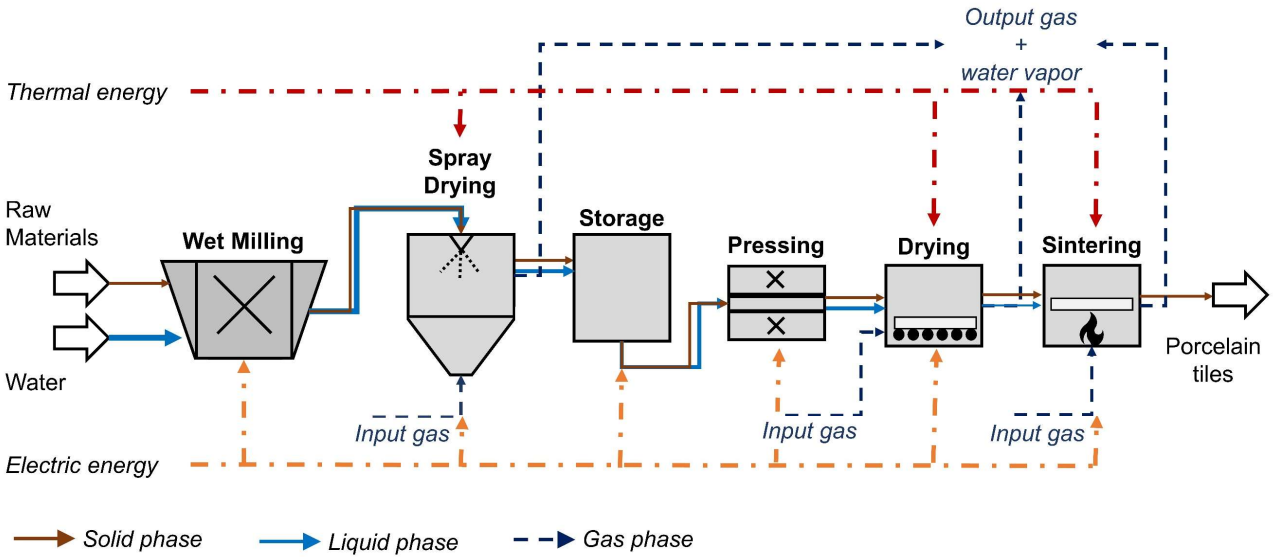

Fig. 1 Flowchart of "wet" route configuration for porcelain stoneware manufacturing with respective energy and material flows.

Even though there are several studies for each single unit operation of the entire plant, integrated studies of the complete processing sequence are scarce. Due to the strong influence of every single unit on the entire process, numerical investigations of such complex plants can be effectively made by flowsheet simulation that treats the process as a whole (1).

In a previous study, a developed flowsheet model implemented in Dyssol framework (2) has been successfully applied for the macroscale modeling of porcelain tile manufacturing, allowing to forecast the behavior of each unit outcome on the subsequent processes throughout the manufacturing sequence. The obtained simulation results were in good agreement with experimental data considering different compositions and processing parameters. This approach enables creating a digital twin of the production, potentially optimizing processing parameters and making a step towards process sustainability (3).

Nevertheless, semi-empirical models applied for each processing unit on the flowsheet simulation have limited reach for various simplifications and assumptions embedded within theoretical solutions development. To tackle this problem and to improve model predictivity discrete element method (DEM) can be used. DEM is a promising approach to understand the dependencies between structural and mechanical properties of granular materials. It takes the particulate structure of the material into account treating each particle individually with all degrees of freedom (4; 5). DEM has been applied in numerous studies for modeling individual ceramics processing steps such as milling, pressing and sintering. Specifically, the bonded-particle model (BPM) is a common approach to simulate the mechanical behavior of agglomerates by specifying the agglomerate structure as a dense pack of spheres connected by bonds (5). Consequently, multi-scale coupling between micro (DEM) and macro scale (flowsheet simulation) holds great potential in achieving the capability to predict the response of porcelain agglomerates during the complete process sequence.

In this paper, the developed BPM-based model was used to obtain further insight into one of the most critical processing steps of tile manufacturing, namely uniaxial pressing. The simulations were validated by experimental analysis considering different material and processing parameters. The validated simulations improved the previous semi-empirical model adopted for the macroscale flowsheet simulation, by refining the independencies of unknown model parameters.

2.0 Material and Methods

The performed experiments were intended to mimic the simulation scenes without size scaling.

2.1 Simulations

All simulations were performed in the open-source DEM simulation framework MUSEN (6). The initial assumption was that the spray dried granules were composed of primary particles (Kaolinite, Quartz and Albite) connected by bonds whose properties depended on the moisture content of the granules, given that the water acts as a plasticizer (7; 8). The soft sphere contact model was employed to describe particle-particle and particle-wall interactions. The normal component of the force was calculated according to the Hertz theory (9) and the tangential component according to the model proposed by Mindlin et al (9). The solid bridge bond model is based on an elastic-plastic model as proposed in (5). The parameters of the primary particles can be seen in

Table 1.

Table 1 Main material parameters of primary particles

Parameter	Value	Reference
Albite as primary particle		
Density	2620 kg/m^3	(10)
Young's modulus	8.5·10^{10} Pa	(11)
Poisson ratio	0.28	(10)
Kaolinite as primary particle		
Density	2520.1 kg/m^3	(12)
Young's modulus	6.2·10^{10} Pa	(13)
Poisson ratio	0.18	(12)
Quartz as primary particle		
Density	2650kg/m^3	(10)
Young's modulus	7.17·10^{10} Pa	(14)
Poisson ratio	0.17	(10)

In the first step, a homogeneous packing of primary particles was generated in a spherical volume with a diameter of 500 μm. Afterward, the bonds were generated between primary particles, with a threshold distance of 80% of particle diameter to ensure full connectivity. The final granule can be seen in Fig. 2a. The numerical analysis was carried out with 50 granules generated in a die of 5 mm diameter, to minimize the number of particles, reducing simulation time. The total amount of bonds was about 2.4 million. The scene simulated can be seen in Fig. 2b. Even though the actual compression velocities are in the range between 0.01 mm/s and 0.1 mm/s, the velocity of the piston in the numerical studies was 0.2 m/s to speed up calculations. The piston speed role was assessed through the creep analysis to evaluate time influence. All simulations were carried up to 60% strain deformation.

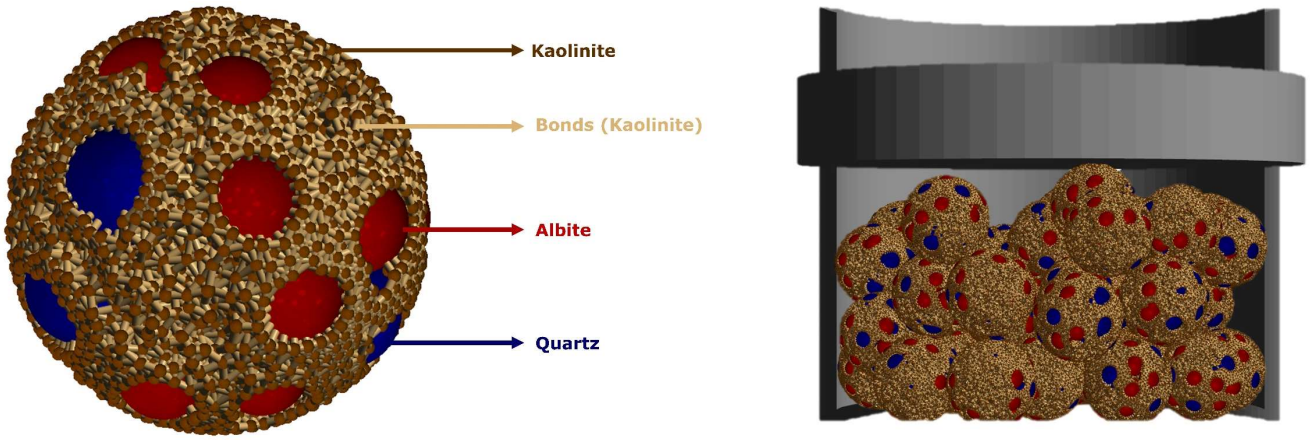

(a) *(b)*

Fig. 2(a) Porcelain granulate generated for numerical analysis (b) Simulation setup for uniaxial pressing

2.2 Experimental Analysis

The composition and particle size distribution of the spray dried porcelain granules used in the porcelain tile manufacturing experiments are listed in Table 2.

Table 2 Composition of the spray dried powder used in the experimental analysis.

	Kaolinite	Albite	Quartz
Mass fraction [%]	25	50	31
SiO_2 [%]	45.03	64.05	99.03
TiO_2 [%]	0.70	-	0.04
Al_2O_3 [%]	38.27	19.72	0.44
Fe_2O_3 [%]	0.54	0.11	0.04
CaO [%]	-	0.20	-
Na_2O [%]	0.12	2.67	-
K_2O [%]	0.04	11.25	0.06
P_2O_5 [%]	0.06	0.17	-
Fire loss [%]	14.00	0.35	0.25
d_{10}[µm]	0.37	2.10	3.48
d_{50}[µm]	2.99	14.45	28.44
d_{90}[µm]	6.48	69.29	81.27

The granules were sieved and the analysis was carried out for the material retained in the 500 µm sieve. Previous analyses of Dynamic Vapor Sorption (DVS) were conducted at 20°C to determine an average moisture content considering room temperature and humidity variations at environmental conditions. The interval of moisture evaluated initially from 1.5 to 8 wt.%, has been extended to 16 wt.% to obtain deeper insight into the mechanical behavior. A climate chamber was used to ensure a homogeneous water content distribution in the prepared samples. After preparation, the samples were left sealed 48h in a climate chamber with saturated humidity to avoid moisture loss to the environment and ensure homogenization.

For every moisture content, 10 runs of 0.14 g-0.16 g of mass of solid materials were examined. All uniaxial pressing experiments were carried out with a Texture Analyzer (TA. XT plus, Stable Micro Systems, Great Britain) using a die of 5 mm diameter and 2.5 cm height with a load cell of 500 N. The velocity was kept constant at 0.1 mm/s. Furthermore, a creep analysis was conducted for samples with different moisture contents keeping the constant strain in the range from 40 to 60% for 1 min to analyze the variation of mechanical behavior over time. The wet density was acquired based on the final strain deformation obtained from the Texture Analyzer and the mass used on every run. Whereas the porosity is calculated based on the initial density of the atomized powder (1 g/cm3) and the green body density attained.

3.0 Results and Discussion

3.1 Experimental Analysis

The analysis of DVS showed that the spray-dried porcelain granules are susceptible to moisture content variations due to relative humidity variation as seen in Fig. 3. Based on the performed creep analysis, no significant creep has been observed,

which allows not to include creep into the model. For further experiments, average relative humidity of 65% was assumed, which would lead to an approximately 1.5 wt.% of moisture content in the granules at ambient conditions.

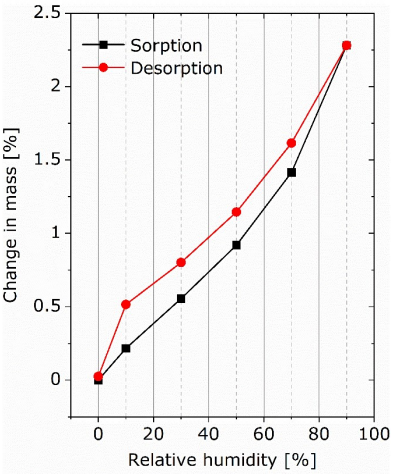

Fig. 3 Dynamic vapor sorption (DVS) analysis of spray dried porcelain granules

Values of moisture content higher than circa 2.5 wt.% are not in equilibrium at ambient conditions. This implication compromises the evaluation of higher moisture content, interfering with the acquisition of accurate moisture content values. Based on this, the samples with different moisture contents could be prepared accordingly for the compression study.

Fig. 4a shows the experimentally obtained curves for the different moisture contents. Each of the curves was obtained after averaging 10 trials. After 30% deformation, it is clear that the higher moisture contents lead to lower stress values indicating lower Young's modulus and increased deformability, which agrees with previous studies (15). For better evaluation and due to the small sample sizes, the experiments were grouped in three groups: below 5 wt.%, between 5 wt.% and 10 wt.% and above 10 wt.%. The grouped moistures can be seen in Fig. 4b.

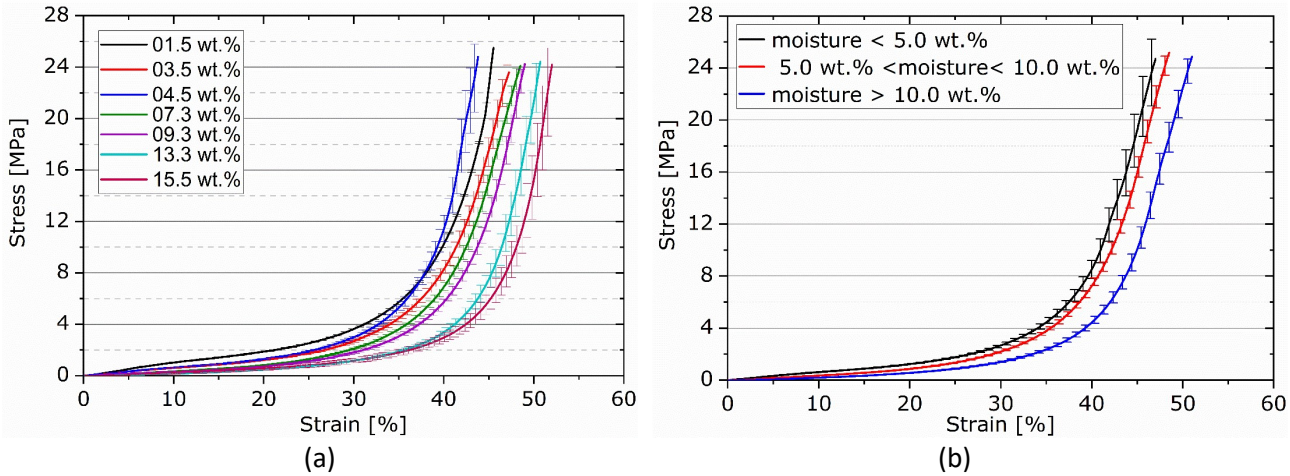

Fig. 4 (a) Average mechanical behavior of compression tests performed on Texture Analyzer for atomized porcelain granules with different moisture contents (b) Mechanical behavior of averaged samples with moisture below 5 wt.%, between 5 wt.% and 10 wt.% and above 10 wt.%

The first derivative of the stress-strain curves, can be seen in Fig. 5. In all evaluations, there is an increase of the response followed by an abrupt decrease. This

response can be interpreted as stiffness during compression of the sample, which could be due to an increase of apparent Young's modulus or friction of the system.

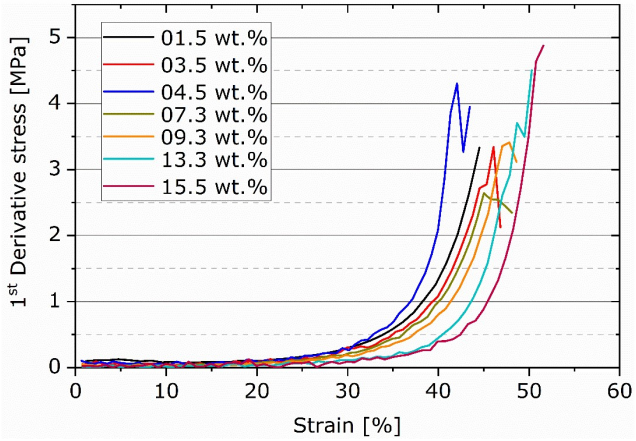

Fig. 5 1st derivative stress behavior of the averaged experimental results

The average wet density after compression (i.e. 25 MPa) of the green bodies and their porosities for every moisture content can be seen in Fig. 6. It is clearly noted that the density of the green bodies increases with higher moisture content whereas there is a decrease of porosity. An increasing moisture leads to higher plasticity in the system that facilitates the rearrangement of particles and reduction of elastic expansion in the system. These factors tend to reduce the volume of pores in higher pressure stresses (15; 16).

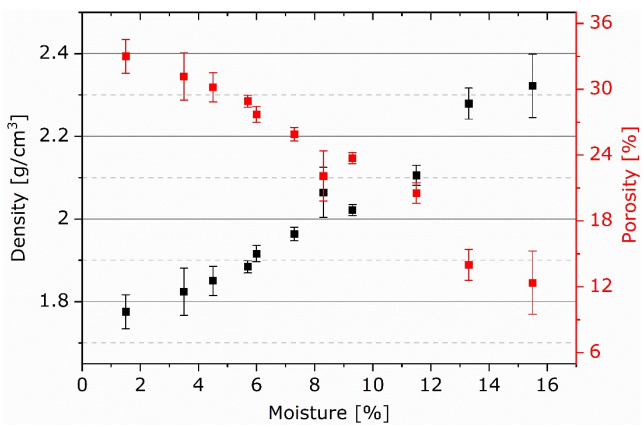

Fig. 6 Wet density values and porosities of the green bodies obtained after uniaxial pressing tests at 25 MPa.

Albaro et al. proposed that the volume of intergranular pores, i.e. the compaction degree, reduces exponentially with the pressure applied during compaction (16). It was also proposed that the ratio of solid and liquid volume correlates with the compaction degree, which in turn can be associated with the final porosity and density achieved (15). Thus, the influence of the moisture on the porosity and the density can be well described with the exponential decay and growth, respectively, as given by (Eq. *1*.

$$y = a \cdot exp(bx) \qquad \text{(Eq. 1)}$$

Table 3 presents the fitted parameters for (Eq. *1* with corresponding goodness of it, indicated by the R-square value. The plotted function with the values of the experiments and 90% prediction bounds can be seen in Fig. 7.

$$y = a \cdot exp(bx) \quad \text{(Eq. 1)}$$

Table 3 Fitted function parameters for density and porosity as a function of moisture

Density		*Porosity*	
a	1.692	a	39.11
b	0.02107	b	-0.06025
R^2	0.97	R^2	0.9

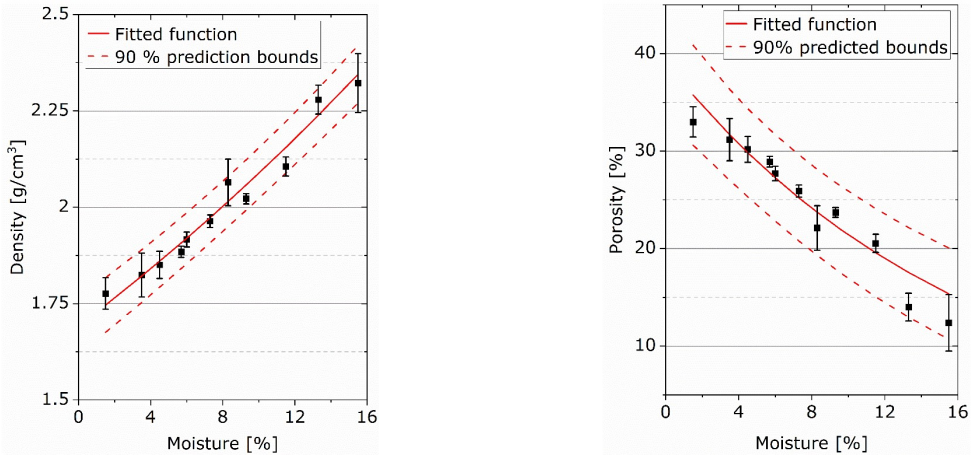

(a) *(b)*

Fig. 7 Green body properties after uniaxial pressing variation with different moisture content and respective fitted function for (a) Wet Density (b) Porosity

3.2 Simulation

The simulation scene before and after compaction can be seen in Fig. 8. The averaged experiments with varied moisture content (s. Fig. 4b) were used as a basis to adjust the unknown model parameters. The estimated model parameters and the properties of solids bonds can be seen in

Table 4. Fig. 9 shows the comparison between simulations and experiments.

(a) *(b)*

Fig. 8 Simulation scene (a) Before compaction (b) After compaction reaching 60% strain deformation

Table 4 Estimated model parameters used for BPM simulation of solid bonds

Main model parameters	Moisture <5wt.%	5wt.%<moisture<10 wt.%	Moisture >10wt.%
Bonds Young's modulus [GPa]	2.0	2.0	2.0
Bonds yield strength [MPa]	2.0	0.9	0.6
Interparticle sliding friction [-]	0.65	0.55	0.45
Poisson ratio [-]	0.184	0.184	0.184
Fracture strain tension [-]	0.5	0.5	0.5

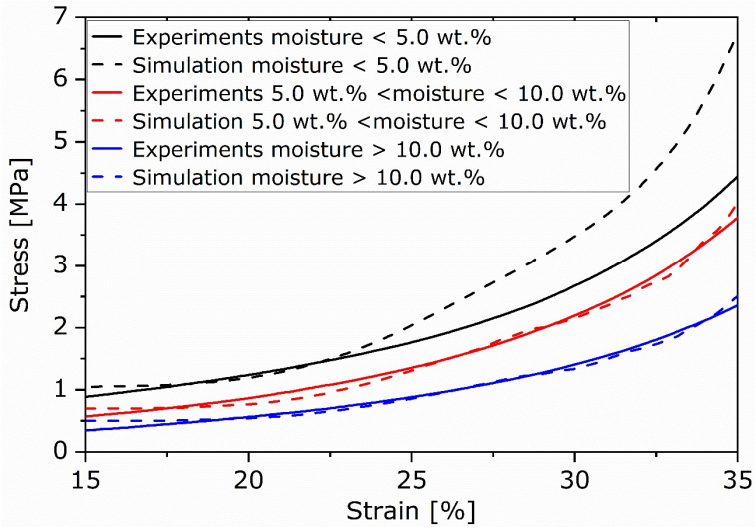

Fig. 9 Comparison of simulation results with experimental data

The granules rearrangement (known as a first compaction mechanism) is not considered in simulation which justifies the offset of the experimental stress-strain curves (16). A good agreement between simulations and experiments has been achieved in the range from 15% to 35% strain. The increased stiffness, as seen in Fig. 5, does not considered in the current model and this compromises the fitting for further deformations. Consequently, it is required to modify the current model to take that into account.

It can be seen that the moisture directly influenced the mechanical behavior of bonds by analyzing the fitted parameters. The increasing moisture content leads to reduced yield strength and decrease of interparticle sliding friction. The trend agrees well with previous studies on the mechanical behavior of clay with varied moisture content (17; 15).

In the experiments conducted, no significant differences could be observed between experimental data and simulations in the moisture range from 3 to 7 wt.% of porcelain tile pressing. Among the reasons could be the small volume of analysed sample which was used in order to be able to perform the simulations one-to-one. For a better description of the mechanics in this range, further analysis has to be carried out considering additional parameters as, for instance, granule size distribution or plastic deformation of primary particles.

4.0 Conclusion and Outlook

Flowsheet simulations are able to establish a digital twin of porcelain tile manufacturing. Still, the empirical or semi-empirical models applied require significant improvement to determine optimal process parameters and to digitalize the entire processing sequence.

In this contribution, further insight has been taken into uniaxial pressing employing experiments and microscale DEM simulations. The experiments showed that the higher moisture content of the samples leads to lower values of elastic stiffness. This fact is even more visible after 30% of strain. The density of the green bodies increased with the moisture content, whereas the porosity decreased. Two simplified correlations were proposed to describe these dependencies.

The simulation results are in good agreement with experimental data for strain in the range between 15% and 35%. The increased stiffness observed constrained the proposed model's applicability since it does not consider a Young's modulus and yield strength variations. Consequently, for a better description, the current model has to be extended to consider variation of the simulation parameters. Moreover, further analysis has to be carried out to consider additional parameters that directly influence the process. With a better description of the conditions used during pressing, the DEM simulations can generate data-driven black-box models to substitute or extend the current semi-empirical model used for the macroscale flowsheet simulations. As a consequence, this will favor the detailed description of the complete processing sequence.

5.0 References

1 DOSTA, Maksym; LITSTER, James D.; HEINRICH, Stefan. Flowsheet simulation of solids processes: Current status and future trends. **Advanced Powder Technology**, v. 31, n. 3, p. 947–953, 2020. doi:10.1016/j.apt.2019.12.015.

2 SKORYCH, Vasyl; DOSTA, Maksym; HEINRICH, Stefan. Dyssol—An open-source flowsheet simulation framework for particulate materials. **SoftwareX**, v. 12, p. 100572, 2020. doi:10.1016/j.softx.2020.100572.

3 ALVES, C. L.; NONI JR, A. de; JANSSEN, R.; HOTZA, D.; RODRIGUES NETO, J. B.; GÓMEZ GONZÁLEZ, S. Y.; DOSTA, M. Integrated process simulation of porcelain stoneware manufacturing using flowsheet simulation. **CIRP Journal of Manufacturing Science and Technology**, v. 33, p. 473–487, 2021. doi:10.1016/j.cirpj.2021.04.011.

4 BESLER, Robert; ROSSETTI DA SILVA, Marcel; DO ROSARIO, Jefferson J.; DOSTA, Maksym; HEINRICH, Stefan; JANSSEN, Rolf. Sintering Simulation of Periodic Macro Porous Alumina. **Journal of the American Ceramic Society**, v. 98, n. 11, p. 3496–3502, 2015. doi:10.1111/jace.13684.

5 SPETTL, Aaron; DOSTA, Maksym; ANTONYUK, Sergiy; HEINRICH, Stefan; SCHMIDT, Volker. Statistical investigation of agglomerate breakage based on combined stochastic microstructure modeling and DEM simulations. **Advanced Powder Technology**, v. 26, n. 3, p. 1021–1030, 2015. doi:10.1016/j.apt.2015.04.011.

6 DOSTA, Maksym; SKORYCH, Vasyl. MUSEN: An open-source framework for GPU-accelerated DEM simulations. **SoftwareX**, v. 12, p. 100618, 2020. doi:10.1016/j.softx.2020.100618.

7 ALBARO, J. A. A operação de prensagem: considerações técnicas e sua aplicação industrial. Parte I: O preenchimento das cavidades do molde. **Cerâmica Industrial**, v. 5, n. 5, p. 23–28, 2000.

8 HORABIK, Jozef; JOZEFACIUK, Grzegorz. Structure and strength of kaolinite–soil silt aggregates: Measurements and modeling. **Geoderma**, v. 382, p. 114687, 2021. doi:10.1016/j.geoderma.2020.114687.

9 HERTZ, H. Über die Berührung fester elastischer Körper. **Journal für die reine und angewandte Mathematik**, v. 92, p. 156–171, 1881.

10 ANTHONY, J. W.; BIDEAUX, R. A.; BLADH, K. W.; NICHOLS, M. C. **Handbook of Mineralogy II. Elements, Silica, Silicates. Mineral Data Publishing**: Tucson, Arizona, 1990.

11 DAL BÓ, Marcelo; CANTAVELLA, Vicente; SÁNCHEZ, Enrique; HOTZA, Dachamir; GILABERT, Francisco A. Fracture toughness and temperature dependence of Young's modulus of a sintered albite glass. **Journal of Non-Crystalline Solids**, v. 363, p. 70–76, 2013. doi:10.1016/j.jnoncrysol.2012.12.001.

12 ANTHONY, J. W.; BIDEAUX, R. A.; BLADH, K. W.; NICHOLS, M. C. **Handbook of Mineralogy. I. Elements, sulfides, sulfosalts. Mineral Data Publishing**: Tucson, Arizona, 1990.

13 HÚLAN, Tomáš; ŠTUBŇA, Igor. Young's modulus of kaolinite-illite mixtures during firing. **Applied Clay Science**, v. 190, p. 105584, 2020. doi:10.1016/j.clay.2020.105584.

14 DAL BÓ, Marcelo; CANTAVELLA, Vicente; SANCHÉZ, Enrique; GILABERT, Francisco A.; BOSCHI, Anselmo O.; HOTZA, Dachamir. An estimate of quartz content and particle size in porcelain tiles from young's modulus measurements. **Ceramics International**, v. 43, n. 2, p. 2233–2238, 2017.

15 ALBARO, J. A. A operação de prensagem: considerações técnicas e sua aplicação industrial. Parte III: Variáveis do Processo de Compactação. **Cerâmica Industrial**, v. 6, n. 1, p. 15–23, 2000.

16 ALBARO, J. A. A operação de prensagem: considerações técnicas e sua aplicação industrial. Parte II: A compactação. **Cerâmica Industrial**, v. 5, n. 6, p. 14–20, 2000.

17 ERGULER, Z. A.; ULUSAY, R. Water-induced variations in mechanical properties of clay-bearing rocks. **International Journal of Rock Mechanics and Mining Sciences**, v. 46, n. 2, p. 355–370, 2009. doi:10.1016/j.ijrmms.2008.07.002.